Dalton Transactions

Accepted Manuscript



This is an *Accepted Manuscript*, which has been through the Royal Society of Chemistry peer review process and has been accepted for publication.

Accepted Manuscripts are published online shortly after acceptance, before technical editing, formatting and proof reading. Using this free service, authors can make their results available to the community, in citable form, before we publish the edited article. We will replace this Accepted Manuscript with the edited and formatted Advance Article as soon as it is available.

You can find more information about *Accepted Manuscripts* in the **Information for Authors**.

Please note that technical editing may introduce minor changes to the text and/or graphics, which may alter content. The journal's standard <u>Terms & Conditions</u> and the <u>Ethical guidelines</u> still apply. In no event shall the Royal Society of Chemistry be held responsible for any errors or omissions in this *Accepted Manuscript* or any consequences arising from the use of any information it contains.



Cite this: DOI: 10.1039/c0xx00000x

www.rsc.org/xxxxxx

ARTICLE TYPE

N-doped TiO₂/C nanocomposite and N-doped TiO₂ synthesised at different thermal treatment temperature with the same hydrothermal precursor

Jia Wang, a Chenyao Fan, Zhimin Ren, Xinxin Fu and Zhiyu Wang*

5 Received (in XXX, XXX) Xth XXXXXXXXX 20XX, Accepted Xth XXXXXXXXX 20XX DOI: 10.1039/b000000x

Hydrothermal precursor was first obtained by isopropyl titanate reacting with tetramethylammonium hydroxide (TMAOH), which acts as a source of nitrogen and carbon. A facile post-thermal treatment was employed to enhance the crystallinity and visible light photocatalytic activity of the as-prepared 10 precursor. The resultant products of post-thermal treatment between 200°C to 700°C display different colours from brown to white. N-doped TiO₂ nanoparticles modified with carbon (denoted N-TiO₂/C) was obtained at 300°C, with the colour of black, while yellow N-doped TiO₂ nanoparticles (denoted N-TiO₂) was obtained at 500°C. X-ray diffraction (XRD), Fourier transform infrared spectroscopy (FTIR), X-ray photoelectron spectroscopy (XPS) were applied to characterize N-TiO₂/C, N-TiO₂ and the evolution 15 process during thermal treatment. The results show that for both N-TiO₂/C and N-TiO₂, nitrogen was doped into the lattice, thus narrowing the band gap and increasing the absorption in the visible light region. Moreover, for N-TiO₂/C, the carbon species modified on the surface and between the nanocrystals enhanced the visible light harvesting and increased the adsorption of dye in the photodegradation measurement. The photocatalytic performance under visible light irradiation is N-TiO₂/C > N-TiO₂ > un-20 doped TiO₂.

Introduction

TiO₂ has become the most widely investigated photocatalyst due to high photo-activity, low cost, low toxicity and good chemical and thermal stability.¹⁻⁴ Titanium dioxide is typically an n-type 25 semiconductor due to oxygen deficiency. There are three crystal morphs for titania, anatase, rutile and brookite. Among them, anatase is the most prevalent crystal morph used as photocatalyst. During the photocatalysis process, irradiating photons with energy greater than the band gap of the semiconductor excites an 30 electron from the valence band to the conduction band. In the case of anatase TiO₂, the band gap is 3.2eV, therefore UV light (≤ 387nm) can be absorbed and utilized. However, UV light composes only 7% energy percentage of the whole solar spectrum. Therefore, it is essential to improve the photo response 35 capability of anatase in order to enhance the photocatalytic efficiency. Various strategies have been adopted for improving the photocatalytic efficiency of TiO2. They can be classified as morphological modifications and chemical modifications. As for morphological modifications, increasing surface area and 40 porosity to adsorb more organic dyes or exposing certain facets which are more chemically stable and active such as [100] and [101] have been investigated.^{6,7} Morphological modifications do not concern about altering the energy band gap while chemical modifications usually do. Chemical modifications 45 accompanied by the introduction of chemical deficiencies, which

is usually conducted by the incorporation of additional components into the TiO₂ or by the incomplete oxidation⁸. Thus, the band gap of anatase changes and the absorption range of light get broadened. The dopants are various, metal⁹⁻¹¹ and non-metal¹², ₅₀ ¹³. For application's sake, non-metal dopants are more feasible due to its cost. Specifically, H-, N-, C-, S-doped titania have been studied recent years, and it has been demonstrated that the doping modification can increase the absorption in the visible range. Hdoped anatase is usually prepared by the hydrogenation process 55 via high temperature treatment in H₂ flow¹⁴ or by H₂ plasma¹⁵. The photocatalytic performances of S-doped anatase is inferior to C-doped and N- doped one as reported by C.Bruda. 16 Therefore, more research has focused on the C- and N- modified titania. However, most studied the effect of single element, C- or N-60 modified TiO₂. ^{13, 16-23} Moreover, the doping of N into the lattice of TiO₂ usually results in the formation of oxygen vacancies in the bulk and these defects can act as recombination centers for carriers to decrease the photocatalytic efficiency. ^{23, 25} In addition, it is rather difficult to obtain TiO2 doping with high nitrogen 65 concentration.

Carbon materials with a large electron-storage capacity and metallic conductivity can accept the photon-excited electrons. Researchers have found that carbon coated TiO2 perform better in photocatalytic degradation of organic dyes due to the carbon 70 promoting the separation of electron-hole pair and absorbing more light.²⁴ Therefore, N-doped TiO₂/C nanocomposite is

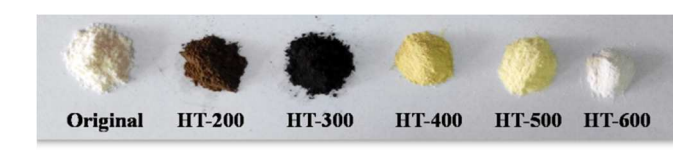


Fig. 1 The products annealed at different temperature

supposed to have higher visible light photocatalytic activity for not only nitrogen dopants improve the optical absorption but also 5 the carbon coating promotes the separation of photoelectrons and holes. An-Wu Xu et al. 25 have confirmed the better photocatalytic performance of N-doped TiO₂/C than N-TiO₂ and TiO₂.

In this study, we develop a novel approach to prepare the C coated, N-doped anatase to improve the visible optical absorption 10 of anatase. We propose a facile synthesis approach without calcinations in specified atmosphere, such as in NH₃ or in an inert atmosphere. In addition, we can control the concentration of dopants with different thermal treatment temperatures, which can be seen clearly from the colour of the products. The 15 corresponding samples illustrate a range of energy band gap from 2.3 to 3.2eV. Photocatalytic measurements were conducted to characterize the photocatalytic activities of N-TiO₂/C and N-TiO₂ by the degradation of methylene blue (MB). N-TiO₂/C displays superior dye-adsorption ability and photocatalytic activity under 20 visible light.

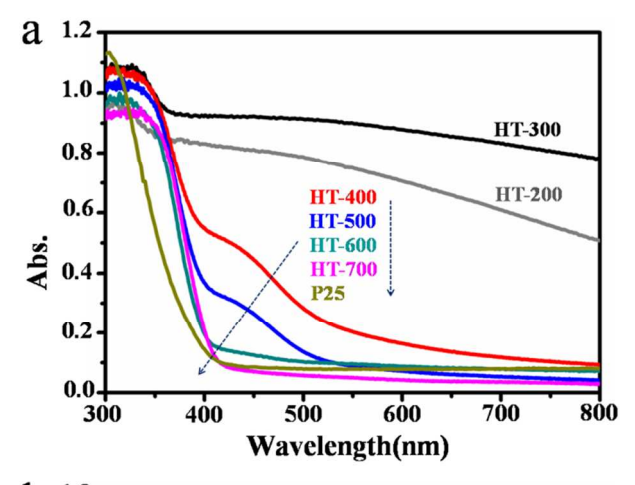
Experimental Section

Synthesis

2mL isopropyl titanate (TTIP) was slowly dipped into 10mL tetramethyl-ammonium hydroxide (TMAOH, 10wt% solution) 25 and 30mL ethylene glycol (EG) to obtain a clear mixture. Then the mixture was transferred to a Telflon-lined stainless steel autoclave with an inner volume of 80mL for hydrothermal treatment at 200°C for 8h. The resultant precipitates were collected and thoroughly rinsed by centrifugation two times with 30 ethanol and deionized water. Finally, the products were dried at 70°C for subsequent thermal-treatment. The dried powders (signed as Original) were calcined under ambient atmosphere for 2h at different temperatures, 200°C, 300°C, 400°C, 500°C, 600°C and 700°C. The corresponding samples are referred to as HT-200, 35 HT-300, HT-400, HT-500, HT-600 and HT-700. The N-TiO₂/C composite and N-TiO2 were prepared by annealing at 300°C and 500°C, respectively.

Characterization

The crystal structures of the Original powders and the HT 40 samples were examined by X-ray diffraction, recorded on a Philips PW1050 X-ray powder diffractometer with Cu-K α (λ = 1.5406Å) from 20° to 80°. The morphological and lattice structural information were characterized by high resolution transmission electron microscopy (TECNAI G2 F20). A 45 spectrophotometer Hitachi U-4100 was used to record the UVvis diffuse reflectance spectra of the samples in the region of 200nm to 800nm. FTIR spectra were recorded on a Nicolet IS10 spectrometer on samples embedded in KBr pellets. Thermogravimetric analysis was performed using a CHNS/O analyzer 50 (PE 2400II, Perkin Elmer, America) in air from room temperature to 800°C with a heating rate of 10K min⁻¹.



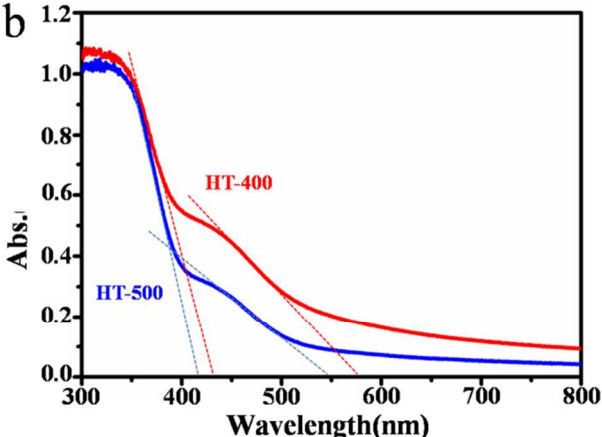


Fig. 2 (a) The UV-Vis diffuse reflectance spectra of all HT samples and P25; (b) The UV-Vis diffuse reflectance spectra of HT-400 and HT-500

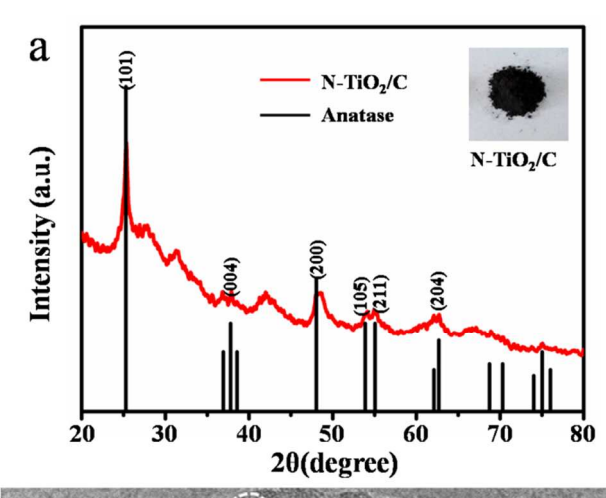
55 Photocatalytic measurements

For photocatalytic degradation experiments, a methylene blue (MB) solution in distilled water was prepared with a concentration of 10mgL⁻¹. 20mg photocatalyst were dispersed in 100mL MB solution in a beaker. The mixture was stirred in the 60 darkness 30min to reach an adsorption-desorption equilibrium between the photocatalyst and MB. Then, the suspension was illuminated by the Xe lamp with output power 50W with visible light range. A filter was used to select the irradiated light range, and only light with λ >400nm could reach the sample. At given 65 time intervals, about 5mL aliquots were sampled, centrifuged. The irradiated solution was kept in ice water to ensure the constant temperature during the photo-degradation process. The residual concentration of organic dye was monitored with a Hitachi U-4100 spectrophotometer.

70 Results and Discussions

The colours of the samples show intuitively information about the effect of thermal treatment at different temperatures in Fig. 1. The Originial powders without heat treatment are lvory white. Others exhibit as addle brown, black, yellow, light yellow and white 75 colour corresponding to HT-200, HT-300, HT-400, HT-500 and

Different colours reflect the different absorption properties in



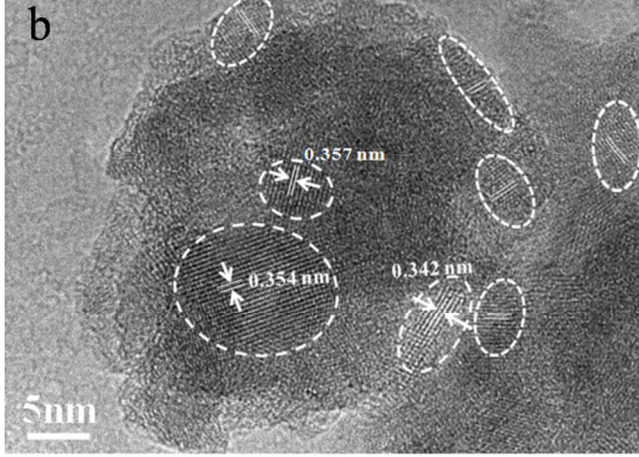


Fig. 3 (a) XRD pattern and (b) HRTEM image of HT-300

visible light region of HT samples. In the UV-vis diffuse reflectance spectra (Fig. 2), commercial P25 reveals an absorption 5 edge around 380nm as expected for anatase TiO2. HT-200 and HT-300 samples absorb in the whole visible region. For HT-400 and HT-500, though the absorption is weak in the visible region, there is a tail in the adsorption edge. The improved absorption can be divided into roughly two parts: 400~450nm (shoulder) and 10 450~680nm (tail) for HT-400, 400~450nm (shoulder) and 450~580nm (tail) for HT-500. The observed "shoulder" and "taillike" features in HT-400 and HT-500 is the typical case for N-TiO₂¹⁵ and accounts for their vellow appearances. At higher annealing temperatures (HT-600 and HT-700), the absorption edge 15 in the UV region becomes more pronounced with the absorption edge around 400nm. It is supposed that with the increase of annealing temperature, the crystallinity of HT samples increased accordingly, accounting for the increasingly clear UV absorption band. The energy gap values calculated from reflectance spectra 20 was displayed in supporting information.

Characterization of HT-300 (N-TiO₂/C nanocomposite)

The black HT-300 sample is actually N-TiO₂/C composite, obtained when annealing the hydrothermal precursor in ambient atmosphere at 300°C for 2h. This temperature allows the 25 formation and co-assembly of carbon species and TiO2 into an interpenetrating TiO₂/C nanoarchitecture and the doping of the nitrogen species into TiO₂.

XRD patterns of the obtained HT-300 nanostructure were collected in Fig. 3 and compared with the standard card of the 30 anatase phase (JCPDS No. 84-1285). The diffraction peaks observed at 20=25.3, 37.9, 48.15, 54.05, and 55.28° are consistent with the standard diffraction data. The broadening of the diffraction peaks is indicative of the small size of the obtained anatase nanocrystals.

HRTEM results illustrated the microstructure of HT-300 composite and presented the existence of carbon. In Fig. 3b, inside the white dotted boxes were crystalline anatase nanocrystals. The HRTEM image shows clear lattice fringes of the nanocrystals with an interplanar spacing of about 0.35nm, 40 which matches well with the (101) plane of anatase TiO₂. The diameter of these TiO₂ crystals is in the range of 3~8nm. It can be concluded from Fig. 3b that the HT-300 sample is composed of crystalline TiO₂ nanocrystals, with the carbon matrix (amorphous) being deposited on the surface and between the 45 nanocrystals.

XPS measurements were used to define the information on the binding energy of a specific element and determined the HT-300 is N-doped, C-coated TiO₂. Fig. 4 compares the XPS spectra of the HT-300 with HT-700. The contrast ample HT-700 is white, 50 anatase phase and obtained by annealing the precursor at 700°C for 2h. The binding energies obtained in the XPS analysis were corrected with reference to the C1s peak (284.6eV). The obvious peaks of carbon, nitrogen, oxygen and titanium can be clearly detected in the survey spectrum (Fig. 4a).

The C1s XPS spectra are displayed in Fig. 4b. Both of the two samples have three main peaks. Two peaks located at 284.6 and 288.4eV are the same for the two samples. The third peak is different, 285.7eV for HT-300 sample and 286.6eV for HT-700 sample. The C1s peak at 284.6eV belongs to the ordered sp² bond 60 of graphite, while the peaks at 286.6 and 288.4eV are ascribed to the existence of C-O and C=O bonds. It is worth noting that the peaks at 285.7eV in HT-300 is attributed to edges, other defects, and disordered carbon, which confirmed the amorphous carbon structure.⁷ The higher intensity of the peaks at 284.6eV and 65 285.7eV in HT-300 in Fig. 3b indicates the higher carbon atomic concentration in the black HT-300 compared with HT-700 sample, and it is supposed that the peak at 284.6eV in HT-700 is adventitious carbon from the internal standard carbon during the XPS measurements.²⁵ No C1s peak at 281eV, which is ascribed to 70 the Ti-C bond, was detected in HT-300, indicating that no carbon dope into the TiO₂ lattice and all carbon species are modified on the surface of TiO2. This result is in accordance with HRTEM result, which shows the HT-300 possesses a TiO₂/C nanocomposite structure.

In Fig. 4c, the relatively high intensity of N1s peak demonstrates the existence of N in HT-300 while there are no distinct peaks observed in HT-700. The relative atomic concentration of N in the N-TiO2/C sample, estimated from the XPS data, was found to be 3.63 atom%. Peaks at 396~398eV can 80 be attributed to the characteristic peaks of the Ti-N-Ti linkage, indicating that the nitrogen atom is substitutionally doped into the TiO₂ lattice. Therefore, the two peaks located at 397.4eV and 397.8eV can be ascribed to the N atoms in TiN crystal.²⁷ However, when a nitrogen substitutes for one oxygen atoms in 85 the initial O-Ti-O structure, the electron density around N in the new O-Ti-N structure is reduced compared with that in a Ti-N-Ti

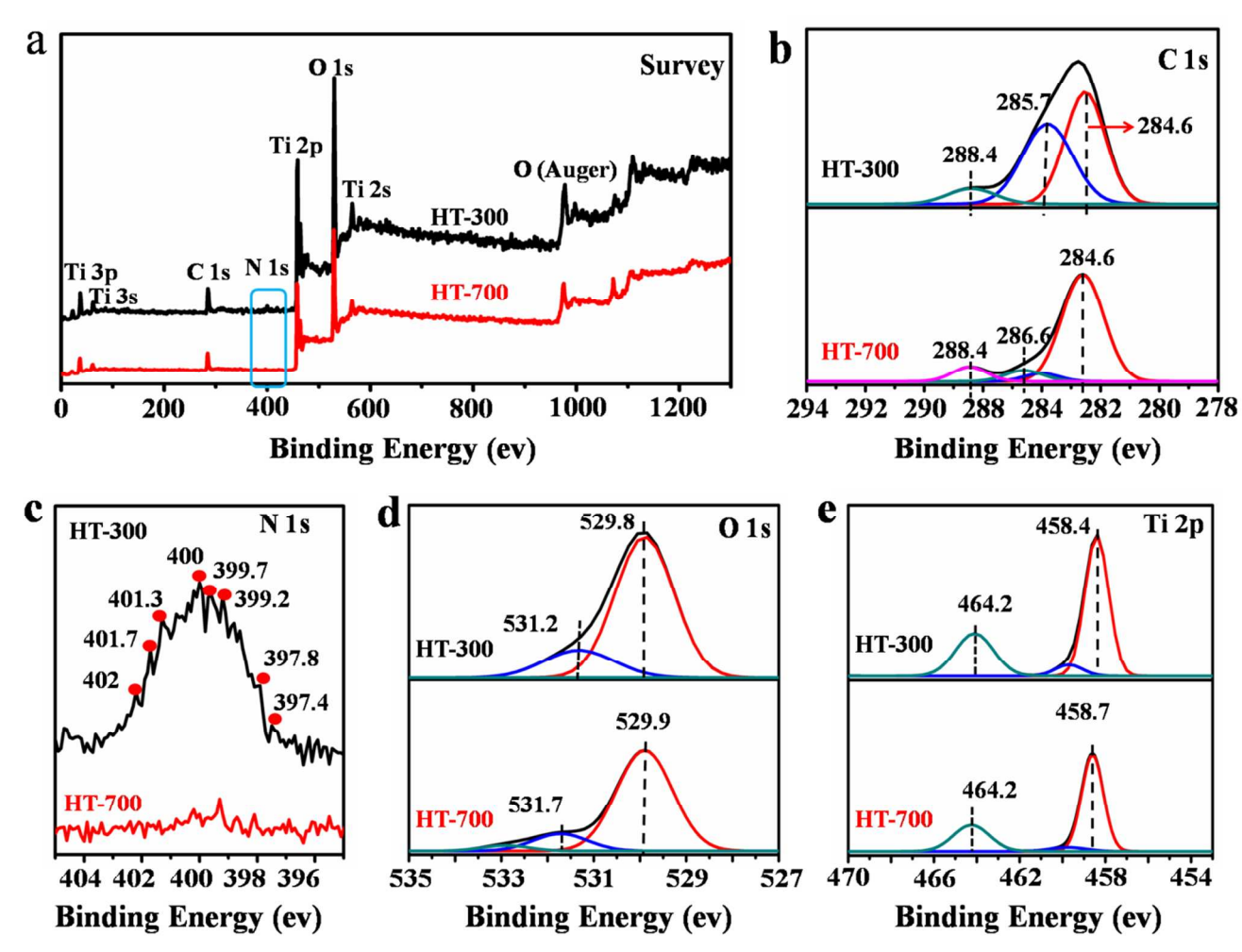


Fig. 4 a) The survey; b) C1s; c) N1s; d) O1s; e) Ti2p XPS spectra of HT-300 and HT-700

structure. Therefore, the peaks at 399.2, 399.7 and 400eV can be attributed to the anionic N in the O-Ti-N linkage. The N1s peaks at 401.3 and 401.7eV can be attributed to the oxidized nitrogen, such as Ti-O-N or Ti-N-O, which may come from the interstitial N in N-TiO₂. Peak 402eV may come from the surface N-H. Therefore, from the atomic N1s XPS spectra, both substitutional (around 397.0eV) and interstitial sites (400.0eV) were observed.²⁷

The O1s peak in the XPS spectrum of HT-300 (Fig. 4d) can be fitted into two peaks centered at 529.8 and 531.2eV. The lower energy peak appearing at 529.8 is attributed to the Ti-O linkage of TiO₂.²² The peak around 531.2 and 531.7eV can be ascribed to -OH groups. The peak intensity of the -OH groups in HT-300 is greater than that in HT-700, for HT-700 was annealed at higher temperature (700°C). Besides, there are no peaks at around 532.2eV, which represent for the formation of oxygen vacancies. As the O 1s peak for the NOx species were at ~533eV, ²⁵ thus, by comparison, the possibility of surface adsorbed nitrogen species can be excluded.

The binding energies of Ti2p_{3/2} and Ti2p_{1/2} for the HT-300 sample are 458.4 and 464.2eV, respectively. The lattice incorporation of nitrogen generates Ti-N bonds by the partial replacement of O anion with N anion, which gives rise to an increase in the electron density on Ti cation because the

electronegativity of the N atom is smaller than the O atom and partial reduction of Ti⁴⁺ to Ti³⁺ occurs, which manifests as a decrease in the Ti2p binding energy. Thus, compared with the control sample, for N-TiO₂/C, a decrease of 0.3eV is observed, indicating the presence of Ti³⁺ and this further confirms that nitrogen is incorporated into the lattice and substitutes for oxygen. ^{25, 27}

From the XPS spectra, HT-300 is confirmed to be N-TiO₂/C, and HT-700 is undoped TiO₂. The possible visible light absorption mechanism for N-TiO₂/C nanocomposites (HT-300) is proposed by An-Wu Xu. ²⁵ The nitrogen incorporation into the crystalline lattice of TiO₂ modifies the electronic band structure of TiO₂, leading to an N-doped level above the O2p valance band, which narrows the band gap of TiO₂ and shifts the optical absorption to the visible light, and the 3d orbital of the Ti³⁺states in TiO₂ forms a donor energy below the conduction band, which also contributes to the visible light absorption in N-doped TiO₂. In addition, when visible light irradiates the surface of N-TiO₂/C nanocomposite, the carbon on the surface can also harvest visible light and enhance the visible light absorption.

Characterization of HT-500 (N-TiO₂)

With the increase of annealing temperature (above 300° C), the

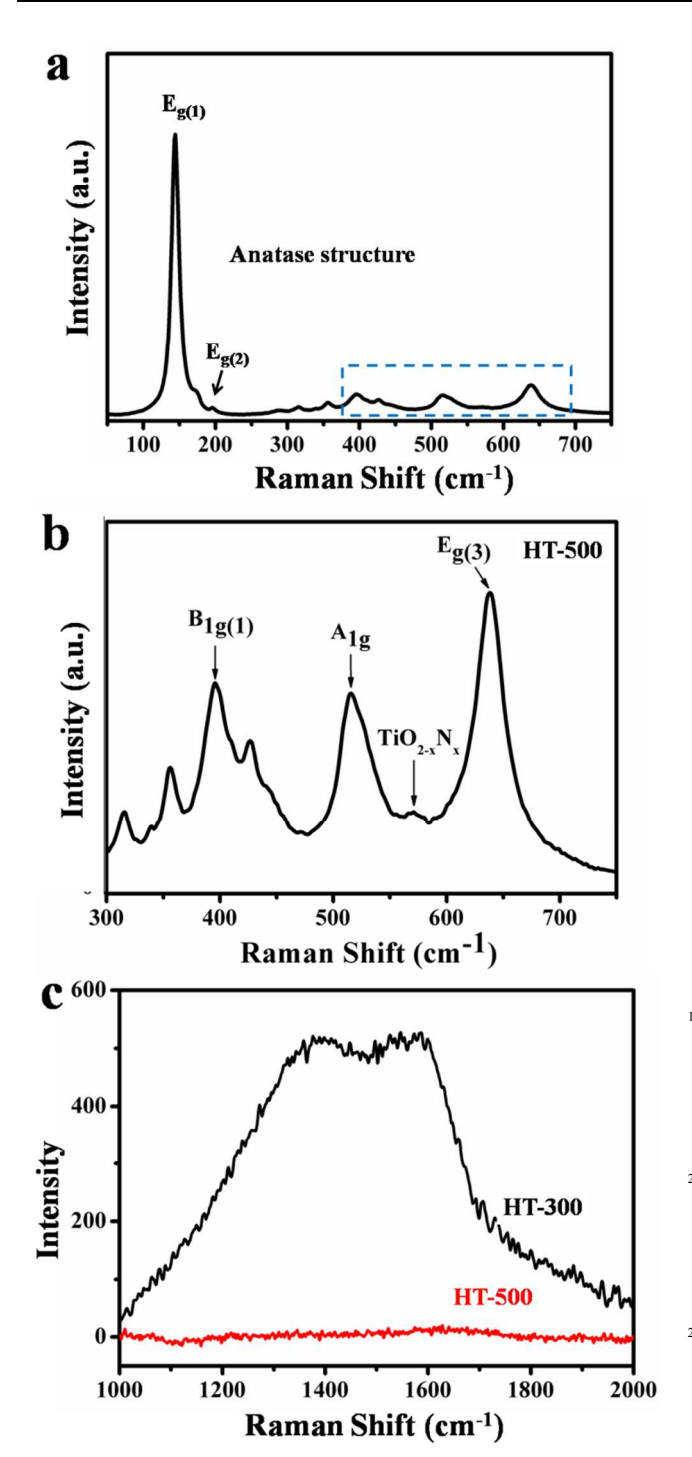
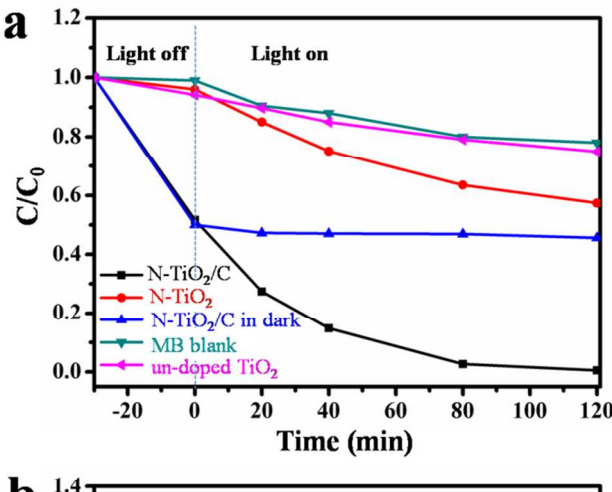


Fig. 5 Raman spectra of the HT-500 sample. (a) Overall Raman spectrum; (b) Enlarged Raman spectrum in the square area marked in (a); (c) Comparison of Raman spectra of the carbon-coated HT-300 (black) and non-carbon coated HT-500 (red)

colour of HT samples became lighter, from black to yellow, the typical colour for N-doped TiO₂. Therefore, it is supposed that the carbon coating in the N-TiO₂/C nanostructure was oxidized under high temperature and the chemical nature of yellow HT-500 is N-10 doped TiO₂. Raman spectroscopy was applied to distinguish the phase of titania and to characterize the carbon in HT-300 and HT-

In general, the Raman peaks around 158 (Eg(1)), 203(Eg(2)),



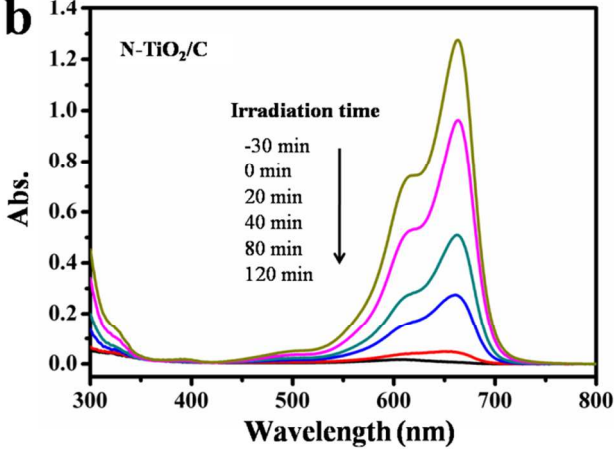


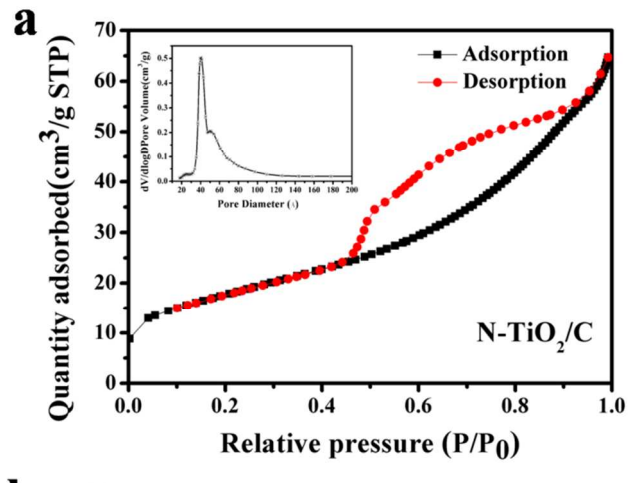
Fig. 6 (a) The photocatalytic degradation of MB over N-TiO₂/C, N-TiO₂ and undoped TiO₂ under visible light; (b) The absorption spectra of the MB solutions with N-TiO₂/C

404(B1g(1)), 512(A1g) and 633(Eg)cm⁻¹ as well as the spectral pattern match well with the results reported in the literature for ₂₀ typical anatase TiO₂ nanocrystals.^{27,28} Fig. 5c compares the Raman spectrum of HT-300 and HT-500 in 1000~2000cm⁻¹. There are two peaks in HT-300; one is at 1592cm⁻¹ corresponding to ordered sp² bond carbon, namely, an E2g mode of graphite, while the other is at around 1357cm⁻¹ is attributed to edges, other 25 defects, and disordered carbon, which confirmed the amorphous carbon structure²⁸. The carbon in HT-300 accounts for the black colour and thermal treatment of residual reactant TMAOH produces these carbon species. However, there no such peaks representing the existence of carbon species in HT-500. Besides, 30 the fitting of the enlarged spectral portion shown in Fig. 5b reveals an additional feature near 560cm⁻¹. This feature can be attributed to the first-order scattering of a nonstoichiometric nitrogen-doped anatase TiO₂ structure.²⁷

Thus, Raman spectra confirm that HT-500 sample is N-doped 35 TiO₂.

Photocatalytic Measurements

The visible-light photocatalytic activities of the samples were characterized by the photodegradation of MB aqueous solution. Fig. 6 shows a comparison of photocatalytic activities of the N-₄₀ TiO₂/C nanocomposites (HT-300), N-TiO₂ (HT-500) and the un-



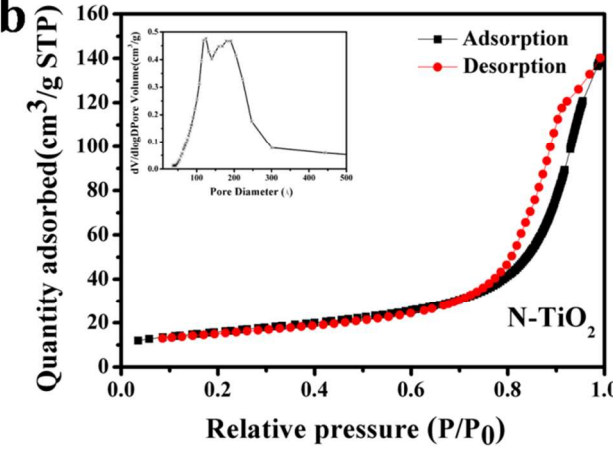
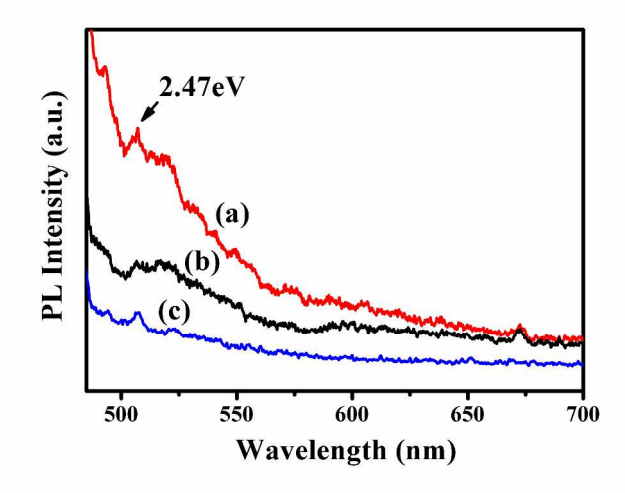


Fig. 7 N₂ adsorption-desorption isotherms and the BJH corresponding pore size distribution curve of (a) N-TiO₂/C and (b) N-TiO₂

doped anatase (HT-700). 20mg photocatalyst was dispersed in 5 100mL 10mg/L MB solution in a beaker. The total concentrations of MB were simply determined by the maximum absorption $(\lambda=664\text{nm})$ measurements. C/C₀ was used to describe the degradation, which stands for the concentration ratio after and before a certain internal. Fig. 6 shows the adsorption and photo-10 degradation of MB under visible light irradiation (λ >400nm) for various photocatalysts. Without irradiation, 48.81%, 2.74%, 1.54% of MB was adsorbed on N-TiO₂/C, N-TiO₂ and un-doped TiO₂ after 30min in darkness, respectively. N-TiO₂/C absorbed the most organic dye in darkness due to the presence of amorphous 15 carbon. As can be seen from the Fig. 6, the un-doped TiO₂ sample also shows a visible light photocatalytic activity. This can be contributed to the degradation of MB on the nanocrystals under visible light due to the self-sensitized degradation of MB.⁷ It can be seen that within 80 min, MB was almost all degraded under 20 visible light irradiation (λ>400nm) when the N-TiO₂/C sample was used as a photocatalyst. Also, Fig. 6 indicates that the N-TiO₂/C sample exhibited superior dye-adsorption and better photocataly-tic activity than N-TiO2, in accordance with the reported results.25

To elucidate the higher absorption of N-TiO₂/C, the N₂ sorption isotherm and the corresponding BJH (Barrett-Joyner-Halenda) pore size distribution curve of the as-prepared N-TiO₂/C and N-TiO₂ are shown in Fig. 7. The surface area and the

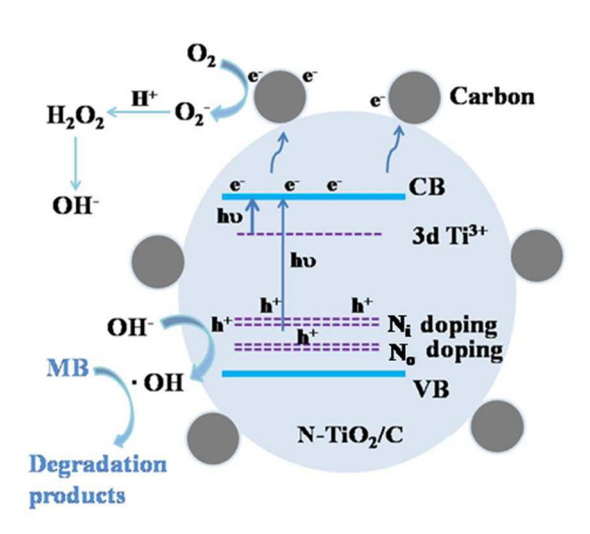


³⁰ Fig. 8 Room temperature photoluminescence (PL) spectra of the samples: (a) N-TiO₂ (HT-500); (b) N-TiO₂/C (HT-300) and (c) un-doped TiO₂ (HT-700)

BJH adsorption average pore diameter of N-TiO₂/C and N-TiO₂ were determined to be 62.8m²g⁻¹, 6.4nm and 55.4m²g⁻¹, 14.6nm 35 respectively. Besides, the hysteresis loop in Fig. 7a appears at a relatively low pressure (0.4<P/P₀<0.9), which implies the N-TiO₂/C has a mesoporous structure with a pore size distribution centered at 6.4nm, whereas the N-TiO2 has a wider pore size distribution centered at 14.6nm. Considering the comparable 40 surface area of the two samples and their different dye adsorption, it is supposed that the much larger degree of adsorption of MB (48.81%) for N-TiO₂/C is ascribed to the mesopores, which are believed to be produced by the agglomeration and connection of adjacent nanoparticles and amorphous carbon.

The surface area is not the only factor that affects the photoactivity of N-TiO₂/C and N-TiO₂. The rate of recombination of e⁻/h⁺ pairs may also be a factor. The photoluminescence (PL) emission spectra were detected and presented in Fig. 8, to elucidate the fate of e⁻/h⁺ pairs in the semiconductor. The excited 50 wavelength was 450nm. The peaks observed in N-TiO₂/C and N-TiO₂ illustrate that the two samples can absorb visible light, while there is no evident peaks in un-doped TiO₂. The peak intensities of N-TiO₂/C are lower than those of N-TiO₂/C, indicating the electron-hole recombination rate of self-trapped excitations in N-55 TiO₂/C was less than in N-TiO₂. [30] In addition, the peak at around 2.47eV is attributed to the oxygen vacancies located at surface (SOVs) [31] and it can be concluded that N-TiO₂ has more oxygen vacancies than N-TiO₂/C. This can be explained by the increase of calcinations temperature. During the annealing 60 process, more oxygen vacancies were produced in N-TiO₂ (HT-500) because the carbon has strong reducibility at high temperature. Therefore, the carbon in N-TiO₂/C improves the light absorption and retards the recombination of photo-generated e⁻/h⁺ pairs.

Scheme 1 illustrates the possible visible light photocatalytic mechanism over N-TiO₂/C nanocomposite. As discussed in the XPS spectra, the N incorporation into the crystalline lattice of TiO₂ result in the N-doping level above the valence band of TiO₂. Besides, N-doping converts some Ti⁴⁺ to Ti³⁺ through charge, 70 which has also been confirmed by the shift of 0.3eV in Ti2p binding energy in Fig. 4(e). Therefore, the band gap of TiO₂ is



Scheme 1 The proposed photocatalytic mechanism over the N-TiO₂ nanocomposites (N_i and N_o represent the interstitial and substitutional nitrogen, respectively)

s narrowed and the optical adsorption shifts to the visible light region. As discussed above in the PL spectra, the carbon on the surface reduces the recombination of photo-generated electrons and adsorbs more light. Through the synergistic effect of N-doping and carbon coating, N-TiO₂/C nanocomposite displays the enhanced visible-light photocatalytic performance.

Exploration of the post-thermal treatment process

Various measurements were applied to explain the evolution process of hydrothermal precursor during the thermal treatment. X-ray diffraction spectra were collected in Fig. 9a to determine 15 the crystal structure and possible phase change during annealing. For samples without calcinations and calcined at below 300°C, no significant diffraction patterns were observed. The samples are likely to be amorphous. For sample Original, the peaks at around 15.6° can be designated to TMAOH, which can be confirmed in 20 FT-IR patterns (Fig. 9b). When the heat treatment temperature increased to 300°C and above, amorphous transferred to anatase. It was found that the HT-400, HT-500, HT-600 and HT-700 products are composed of pure anatase TiO₂ (JCPDS, file No. 84-1285). The diffraction peaks were observed at $2\theta=25.3$, 37.9, 25 48.15, 54.05 and 55.28° and are assigned as (101), (004), (200), (105), and (211) reflectance planes. The intensities of all peaks increased as the temperature increased, indicating the enhancement of the crystallinity. The average particle size was calculated by using the Scherrer equation. The crystal sizes 30 estimated from the (101) peaks show that anatase crystallites in HT-400 and HT-700 are 15.5nm and 18.9nm, respectively. With the increase of annealing temperature, the crystallites' sizes increase slightly.

The typical phase transformation from anatase to rutile occurs at around 600°C. However, in the present study we observed that the anatase phase is sustained at 700°C, which is above the usual transformation temperature. According to our interpretation, this is because of the carbon and nitrogen present around the $\rm TiO_2$ nanoparticles which may suppresses the phase transformation. 40 Similar results were reported by Inagaki et al. 16

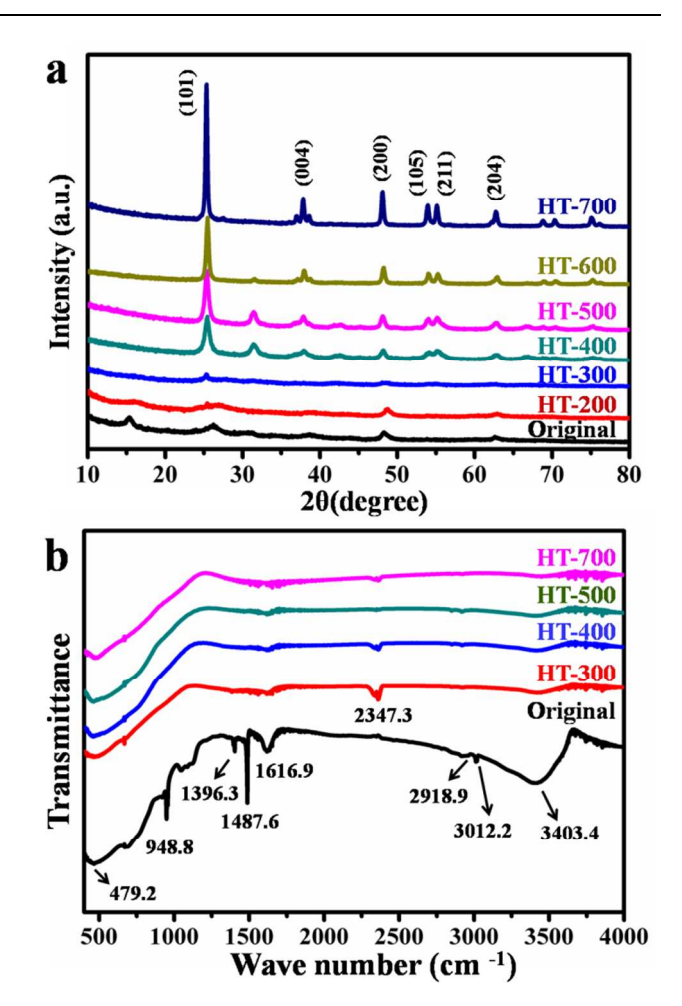


Fig. 9 (a) XRD patterns and (b) FT-IR spectra of the obtained HT samples calcined at different temperatures.

The bonds characteristics of functional groups in the as-45 prepared samples were identified by the FT-IR spectroscopy. Various factors may influence the shape of the FT-IR spectrum, for example, the degree of crystallinity, morphology of the particles. Fig. 9b summarizes the FT-IR spectrum of the Original sample, HT-300, HT-400, HT-500 and HT-700 samples. For the 50 pattern of Original sample, the peak at 3403.4 cm⁻¹ is assigned to the stretching vibration mode of adsorbed water and hydroxvls on the surface of products, and the peak appearing at 1616.9 cm⁻¹ is attributed to the bending vibration of the O-H bond in hydroxyls and adsorbed water. 19, 29 The strong intensities of the peaks at 55 3403.4 and 1616.9cm⁻¹ indicate a high content of adsorbed water and hydroxyls in the Original sample. And it is obvious in Fig. 7b that after thermal treatment, the intensities of peaks at 3403.4 and 1616.9cm⁻¹ weaken greatly. The FTIR spectrum also shows the main bands at 400~700cm⁻¹, which are attributed to Ti-O 60 stretching and Ti-O-Ti bridge stretching modes. 19,30 With calcination, those peaks in samples HT-300, HT-500 and HT-700 are intensified which demonstrates the crystallinity increased with thermal treatment. Compare the IR bands of Original sample with HT samples, the biggest difference lies in the range of 65 900~2100cm⁻¹. Original samples exhibit the intense antisymmetric and symmetric C-H stretching vibrations (at 2918.9cm⁻¹ and 2850cm⁻¹, respectively) of the TMAOH.¹⁹ The shoulder at 2960cm⁻¹ can be associated with the asymmetric

stretching of the terminal -CH₃ groups. The peaks of TMAOH disappear in the HT samples. For the three HT samples, the peaks at 2347.3cm⁻¹ can be detected as carbon-nitrogen bonds and the intensity of the peaks decreased as the calcinations temperature 5 increased. There is no signal of adsorbed -NH3 molecules at 1400cm⁻¹ or hyponitrite at 1385cm^{-1.29} These results are in accordance with the XPS analysis in Fig. 4.

FT-IR patterns show that residual reactant TMAOH was in the surface of original sample. During thermal treatment, TMAOH 10 experienced pyrolysis process. The methyl groups carbonized at 200°C~300°C, contributing to the carbon on the surface and between the crystals in N-TiO₂/C (HT-300), while ammonium groups acted as nitrogen source, providing substitutional and interstitial nitrogen incorporating into N-TiO₂/C and N-TiO₂. 15 Therefore, TMAOH did not exist in samples HT-300 and samples annealed at temperatures above.

In addition, thermo-gravimetric analysis and differential thermal analysis were taken to unveil the revolution of the hydrothermal precursor during the thermal treatment and the 20 results were displayed in Fig. S4. Two stages, the carbonization of residual reactant and the oxidation of carbon species can be clearly observed from the TGA/DTA results, confirming the proposed revolution mechanism of HT samples.

Conclusions

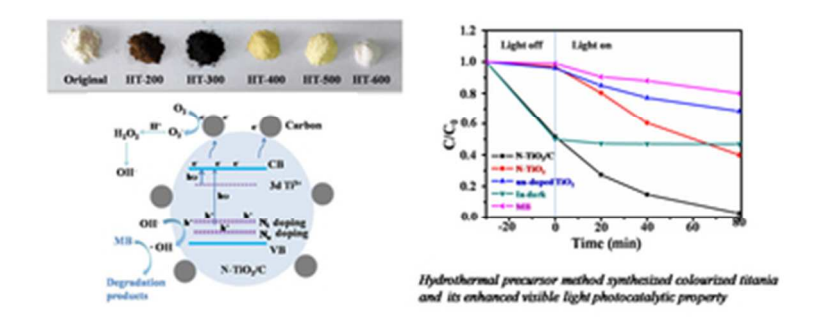
25 In summary, N-TiO₂/C nanocomposites and N-TiO₂ have been successfully prepared by the hydrothermal precursor method. Hydrothermal precursor is actually amorphous titanate with TMAOH residuals. During the post thermal treatment, TMAOH acts as N-doping source and C-coating source. At 300°C and 30 500°C, the calcined samples are proved to be N-TiO₂/C nanocomposite and N-TiO2 and the N content in N-TiO2/C and N-TiO₂ are 2.93 and 2.56 atom%, respectively. The doped nitrogen are in the form of both substitutional nitrogen and interstitial nitrogen, which leads to the generation of Ti³⁺ binding 35 energy level and contributes to the visible light response of the N-TiO₂/C and N-TiO₂ materials. The as-prepared N-TiO₂/C has been demonstrated to be highly active photocatalysts under visible light irradiation. The possible visible light photocatalytic mechanism has been discussed, which can be ascribed to the 40 synergistic effect of visible-light absorption through N-dopants and the restricted recombination of photo-generated carriers with the help of carbon coating. According to the proposed mechanism, the reason why N-TiO₂ performs inferior to N-TiO₂/C is due to the more recombination of carriers without 45 carbon acting as electron- accepter. Moreover, the carbon species act as surface sensitizers and reduce light reflection, which also contributes to the high photocatalytic activity.

Our results provide evidence that the carbon in the N-TiO₂/C can facilitate its photocatalytic activity under visible light by 50 keeping the high reactivity of the photo-generated electrons and holes. This study provides a novel precursor method to synthesize N-doped TiO₂ modified by C components with high nitrogen concentration. Besides, N-doped TiO₂ without carbon was also obtained with the same precursor. It is expected that the 55 hydrothermal precursor method will shed light on the preparation of doping materials modified with carbon, such as S-TiO₂/C and P-TiO₂/C, improving the visible-light photocatalytic activity of TiO2.

Notes and references

- 60 a Department of Materials Science and Engineering, Zhejiang University, Hangzhou, P. R. China. Fax: +86-0571-87951234; Tel: +86-0571-87952334; E-mail: wangzhiyu@zju.edu.cn
 - Address, Address, Town, Country. Fax: XX XXXX XXXX; Tel: XX XXXX XXXX; E-mail: xxxx@aaa.bbb.ccc
- 65 † Electronic Supplementary Information (ESI) available: [details of any supplementary information available should be included here]. See DOI: 10.1039/b000000x/
- ‡ Footnotes should appear here. These might include comments relevant to but not central to the matter under discussion, limited experimental and 70 spectral data, and crystallographic data.
- 1. A. Fujishima and K. Honda, Nature, 1972, 238, 37-+.
- S. K. Das, M. K. Bhunia and A. Bhaumik, Dalton Transactions, 2010, 39, 4382.
- 3. S. U. M. Khan, M. Al-Shahry and W. B. Ingler, Science, 2002, 297, 2243-2245.
- C. Liu and S. Yang, ACS Nano, 2009, 3, 1025-1031. 4.
- K. B. Jaimy, V. P. Safeena, S. Ghosh, N. Y. Hebalkar and K. G. K. Warrier, Dalton Transactions, 2012, 41, 4824
- 6. N. Wu, J. Wang, D. N. Tafen, H. Wang, J.-G. Zheng, J. P. Lewis, X. Liu, S. S. Leonard and A. Manivannan, Journal of the American Chemical Society, 2010, **132**, 6679-6685.
- Z. Wang, C. Yang, T. Lin, H. Yin, P. Chen, D. Wan, F. Xu, F. Huang, J. Lin, X. Xie and M. Jiang, Energy & Environmental Science, 2013, 6, 3007.
- J. Yu, G. Dai, Q. Xiang and M. Jaroniec, Journal of Materials Chemistry, 2011, 21, 1049.
- W. Choi, A. Termin and M. R. Hoffmann, Angewandte Chemie, 1994, 106, 1148-1149.
- 10. M. A. Khan, S. I. Woo and O. B. Yang, International Journal of Hydrogen Energy, 2008, 33, 5345-5351.
- 11. M. A. Aramendía, V. Borau, J. C. Colmenares, A. Marinas, J. M. Marinas, J. A. Navío and F. J. Urbano, Applied Catalysis B: Environmental, 2008, 80, 88-97.
- 12. T. Lin, C. Yang, Z. Wang, H. Yin, X. Lü, F. Huang, J. Lin, X. Xie and M. Jiang, Energy & Environmental Science, 2014, 7, 967.
- 13. Y. Li, D.-S. Hwang, N. H. Lee and S.-J. Kim, Chemical Physics Letters, 2005, 404, 25-29.
- 14. G. Wang, H. Wang, Y. Ling, Y. Tang, X. Yang, R. C. Fitzmorris, C. Wang, J. Z. Zhang and Y. Li, Nano Letters, 2011, 11, 3026-3033.
- 100 15. Z. Wang, C. Yang, T. Lin, H. Yin, P. Chen, D. Wan, F. Xu, F. Huang, J. Lin, X. Xie and M. Jiang, Advanced Functional Materials, 2013, 23, 5444-5450.
 - 16. X. Chen and C. Burda, Journal of the American Chemical Society, 2008, 130, 5018-5019.
- 105 17. F. Spadavecchia, G. Cappelletti, S. Ardizzone, C. L. Bianchi, S. Cappelli, C. Oliva, P. Scardi, M. Leoni and P. Fermo, Applied Catalysis B: Environmental, 2010, 96, 314-322.
 - 18. C. Randorn and J. T. S. Irvine, Journal of Materials Chemistry, 2010, **20**. 8700-8704.
- 110 19. H. Li, D. Wang, H. Fan, P. Wang, T. Jiang and T. Xie, Journal of Colloid and Interface Science, 2011, 354, 175-180.
 - Y. Zhao, Y. Li, C.-W. Wang, J. Wang, X.-Q. Wang, Z.-W. Pan, C. Dong and F. Zhou, Solid State Sciences, 2013, 15, 53-59.
- 21. V. Etacheri, M. K. Seery, S. J. Hinder and S. C. Pillai, Chemistry of Materials, 2010, 22, 3843-3853.
- 22. G. Yang, Z. Jiang, H. Shi, T. Xiao and Z. Yan, Journal of Materials Chemistry, 2010, 20, 5301-5309.
- 23. B. Tian, Y. Qian, B. Hu, J. Sun and Z. Du, Journal of Materials Research, 2012, 27, 2408-2416.
- 120 24. R. Asahi, T. Morikawa, T. Ohwaki, K. Aoki and Y. Taga, Science, 2001, **293**, 269-271,
 - 25. D.-H. Wang, L. Jia, X.-L. Wu, L.-Q. Lu and A.-W. Xu, Nanoscale, 2012, 4, 576-584.
- 26. S. Shanmugam, A. Gabashvili, D. S. Jacob, J. C. Yu and A. Gedanken, Chemistry of Materials, 2006, 18, 2275-2282.

- 27. H. Wu and Z. Zhang, International Journal of Hydrogen Energy, 2011, 36, 13481-13487.
- 28. Z. Ren, C. Chen, X. Fu, J. Wang, C. Fan, G. Qian and Z. Wang, Materials Letters, 2014, 117, 124-127.
- 5 29. F. Dong, S. Guo, H. Wang, X. Li and Z. Wu, The Journal of Physical Chemistry C, 2011, 115, 13285-13292.
- 30. C.-Y. Yen, Y.-F. Lin, C.-H. Hung, Y.-H. Tseng, C.-C. M. Ma, M.-C. Chang and H. Shao, Nanotechnology, 2008, 19, 045604.
- 31. F. Dong, S. Guo, H. Wang, X. Li and Z. Wu, The Journal of Physical Chemistry C, 2011, 115, 13285-13292.



32x12mm (300 x 300 DPI)